2024 IEEE/RSJ International Conference on Intelligent Robots and Systems (IROS)
IEEE Robotics and Automation Letters (RAL) paper presented at
October 14-18, 2024, Abu Dhabi, UAE
2024 IEEE/RSJ International Conference on Intelligent Robots and Systems (IROS)
October 14-18, 2024. Abu Dhabi, UAE

Advanced Enhanced Control of a Novel Wearable Lower-Limb Exoskeleton

Shuang Qiu, Zhongcai Pei, Jia Shi, Xu Zhang, Chen Wang, Zhiyong Tang

***Abstract*—In this paper, a novel powered lower limb exoskeleton prototype called PTEXO for reducing user burden and enhancing following comfort is presented. The PTEXO is designed with a new control strategy, Enhanced Sensitivity Amplification Control (ESAC), and improves comfort of lower-limb locomotion through three aspects, namely, obtaining high-quality angular acceleration signals, adjusting sensitivities among different model items, and increasing continuity during gait phase transitions. This opens a new option in terms of algorithms for improving the comfort of wearable robotic exoskeletons. In the paper, the mechatronic structure of PTEXO is designed for ESAC, with which dynamic models are established. Finally, wearable experiments validate the proper functioning of the integrated technique, demonstrating the effectiveness of the ESAC strategy in improving PTEXO smoothness. A user survey is included to illustrate the ESAC can effectively and comfortably assists users with lower limb locomotion.**

***Index Terms*—Wearable Robotics; Force Control; Physical Human-Robot Interaction**

I. Introduction

A robotic exoskeleton is a wearable device worn by humans and can be attached to human limbs to complete the work together with the movement. It is mainly composed of a frame worn outside the human body and a power system. It is characterized by relying on the power system to help human limb joints and muscle movement, which is used to enhance, extend, compensate or replace human limb functions and capabilities [1], such as enhancing human performance, increasing endurance, and assisting the disabled and the elderly in their movements. The applications of the lower limbs are more abundant than those of the upper limbs [2], because they are all related to the walking function of human beings: on the one hand, walking bipedally and upright is a manifestation of human beings distinguishing themselves from other animals, and is also a prerequisite for liberating human hands to create and use tools and prompting the brain to continuously evolve; on the other hand, human beings want to break through the limits of the lower limbs, such as strength, speed, endurance and so on, in order to realize the needs of operations in their specialized fields [3].

There is extensive research on robotic exoskeletons, but controlling them remains a challenge [4], [5]. This is particularly true in scenarios where exoskeletons need to interact with people and the environment in a friendly way [6], especially in the field of augmented lower limb locomotion. One of the main challenges in designing and controlling powered exoskeletons is to maintain the user's natural behaviors when interacting with the exoskeleton [7]. In other words, the worn exoskeleton should not hinder lower-limb locomotion, namely, enhance the user's experience, and ideally should be “invisible” to the user. An ideal “invisible” exoskeleton would follow the user's movements without generating interaction forces. So, minimizing the forces involved in human-exoskeleton interaction is crucial. This necessitates further development in the control strategies of robotic exoskeletons [8], [9].

Assistive strategies for setting control goals heavily rely on sensors. Joint angle sensors [10] and plantar pressure sensors [11] are widely used in both medical rehabilitation and power-assisted exoskeletons. More advanced but less widely used solutions include Electroencephalogram (EEG) [12], Electrooculography (EOG) [13], and surface Electromyography (EMG) [14], [15]. Nevertheless, these sensors are typically complicated to calibrate, prone to interference, and have limited reliability, often require high learning costs, and necessitate constrained wearing. Therefore, it is necessary to investigate control strategies that are less dependent on sensors.

In terms of enhance the strength and performance of human lower limbs control algorithms, the best-known control strategy is Sensitivity Amplification Control (SAC) [16], which is originally proposed for BLEEX [17] and is also used in the control practices of XOS [18], HULC [19], and HLEER [20]. SAC defines the wearer torque acting on the exoskeleton as a sensitivity transfer function, and then amplifies that function to enable the control of exoskeleton with less force. This control method establishes a mapping relationship between the equivalent wearer torque and the kinematic variables of the exoskeleton, creating a new upper-level closed-loop feedback system. The SAC strategy changes the reliance of the exoskeleton control system from sensors to models. By utilizing the information from the existing model and employing the sensitivity amplification control algorithm, the number of sensors required in the exoskeleton control system is minimized. This control strategy has been extensively researched and implemented in the field of robotic exoskeletons.

However, the traditional SAC faces practical application challenges with the following problems: a) Directly calculating the angular acceleration of a joint using the differential method can make it challenging to obtain

Manuscript received: September 7, 2023; Revised: March 10, 2024; Accepted: April 30, 2024. This paper was recommended for publication by Editor Jee-Hwan Ryu upon evaluation of the Associate Editor and Reviewers' comments. This work was supported by the National Nature Science Foundation of China under grant 51075017. *(Shuang Qiu and Jia Shi and Xu Zhang contributed equally to this work.) (Corresponding author: Shuang Qiu.)*

Shuang Qiu, Zhongcai Pei, Chen Wang, and Zhiyong Tang are with the Beihang University, Beijing, China. (email: qiushuang@buaa.edu.cn, peizc@buaa.edu.cn, venus@buaa.edu.cn, zyt_76@buaa.edu.cn).

Jia Shi is with the Beihang University, and also with the CITIC Securities Company Limited, Beijing, China. (email: shijia1@buaa.edu.cn).

Xu Zhang is with the Beijing Legendary Soaring Technology Company Limited, Beijing, China. (email: 748745067@qq.com).

Digital Object Identifier (DOI): see top of this page.

high-quality angular acceleration signals; b) The control system is more responsive to changes in acceleration than velocity. Using a single amplification factor for both the inertial force term and the centrifugal force and Coriolis force term in the control system is not an optimal solution; c) Traditional SAC commands based on inverse dynamics models for the swing phase and stance phase of one leg, respectively. However, this approach leads to sudden and discontinuous changes in control commands during gait phase switches. This instability in the control system leads to sudden changes in forces on the joints, which diminishes the overall wearing experience.

To cope with the above problems, we integrated the tracking differentiator, investigated the fine-grained sensitivity and gait switching factor problems of the system, and proposed Enhanced Sensitivity Amplification Control (ESAC) to enhance the wearing experience. In this paper, the main contributions are summarized as: 1) We developed a novel assisted exoskeleton robot called PTEXO. 2) We developed a new dynamic model for PTEXO. 3) We propose an improved assist control strategy, ESAC, based on the traditional SAC strategy, which can be well adapted to any gait changes. This strategy can solve the issue of auxiliary torque jitter and sudden torque changes during gait switching in a power-assisted exoskeleton, and eliminate the need for additional sensors, thereby enhancing the device's smoothness and reliability.

The remainder of this paper is organized as follows: Section II presents the modeling of PTEXO system based on a novel mechanical design; Section III describes the design of the ESAC strategy based on SAC; Section IV describes the experiment and results discussion; Section V concludes the paper.

II. Design and Modeling of Wearable Exoskeleton

A. Mechatronics Design Concept

The overall electronic control hardware deployment scheme of the PTEXO and the physical object are shown in Fig. 1. Waveshare's Inertial Measurement Unit (IMU) is installed on the torso of the exoskeleton to detect the angle and angular velocity of the torso. MINTASCA's Smart Compliant Actuators (SCA) with integrated magnetic encoders is selected for the four-active degree of freedom joints to measure the angle, angular velocity and provide driving torque. SIMBA TOUCH's plantar pressure sensors are installed in the feet for gait event detection [21]. The Microcontroller Unit (MCU), a Texas Instruments TMS320C2000 series model F28335, is installed on the backplane of the torso section, along with the corresponding peripheral circuits. The lower limb exoskeleton system utilizes the resistive touch serial screen of Guangzhou Dacai Optoelectronic Technology to implement adjustment commands, including motor torque commands and dynamic model parameter adjustment commands. The lower limb exoskeleton robot is powered by TOPGUN's lithium iron phosphate battery. The battery is installed in the main beam of the robot's torso. The straps are made by B&W International GmbH, Germany.

Lower limb exoskeleton robots should follow human-centered design principle. Specifically, the joint distribution of an exoskeleton needs to be consistent with the human lower limb, with all movable joints active to maximize compliance with human limb movement. Exoskeleton in reference [22] meets the above requirements, but the weight of nearly 60kg makes it bulky and complex. In contrast, the total weight of PTEXO designed by us is only 28kg, and its structure has the following characteristics: a) PTEXO is an exoskeleton consisting of 7 rigid linkages with 2 active degrees of freedom (hip and knee flexion/extension) and 4 passive degrees of freedom (hip adduction/abduction and intorsion/extorsion, ankle dorsiflexion/extension and intorsion/extorsion) per leg for locomotor flexibility. b) In order to minimize the overall mass and rotational inertia of each link's end, the battery and weight are designed to be positioned dorsally, with no additional weight added to the ankle joint. Additionally, lightweight foot covers and aluminum alloy materials are used to construct the main structure. c) Designed with adjustable linkage structures for both hip distance, thigh and shank lengths in order to accommodate different body types. As shown in Fig. 2: The hips, thighs and shanks are designed with quick-release locking buckles that allow for continuous and level-less adjustment of the sizes. d) The same type of motor is used for both the hip and knee joints to ensure that the center of mass of the connecting rod aligns with the line between the axes of the two adjacent joints.

Fig. 1. PTEXO's electronic control hardware deployment scheme.

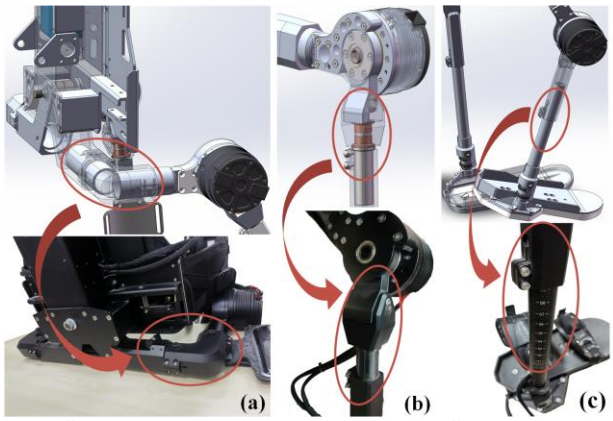

Fig. 2. Adjustment structure of PTLABEXO: (a) Hip adjustment structure (b) Thigh length adjustment structure (c) Shank length adjustment structure.

B. Modeling

Walking is a common form of human locomotion. Normal human walking involves cyclic movements of both legs of the lower limbs. A complete cycle of movement, known as the Gait Cycle [23], is measured by taking one leg as a reference.

The designed PTEXO has four active degrees of freedom and aids only in the sagittal plane. Therefore, its motion and forces in the sagittal plane are the only ones considered when modeling. The model in the sagittal plane can be simplified to a planar five-link model, as depicted in Fig. 3. The projected positions of the two hip joints of the lower limb exoskeleton robot in the sagittal plane are coincident with each other. In order to clearly represent the tandem nature of the lower limb exoskeleton multi-linkage mechanism in the schematic diagram, the joints of rods 2, rods 3, and rods 4 are plotted separately. However, the actual distances of these joints in the sagittal plane are negligible.

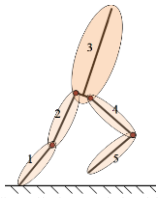

Fig. 3. The equivalent five-link model of lower limb exoskeleton.

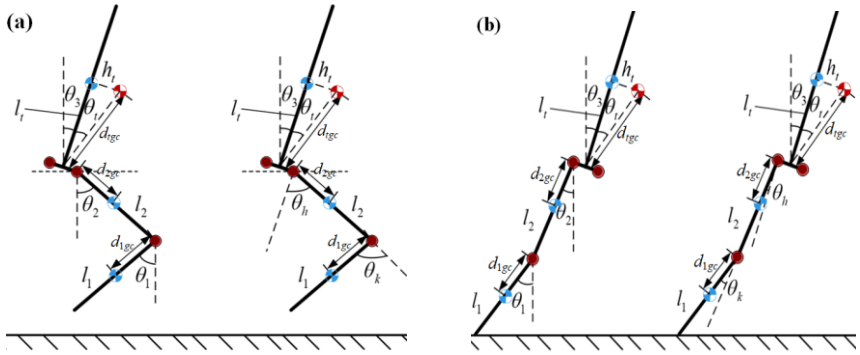

Fig. 4. Diagram of the gait phase model: (a) Swing phase model. (b) Stance phase model. Gravity center of each rod is marked with a blue semicircle. The assumed gravity center is marked with a red semicircle.

l_1 represents the length of rod 1, l_2 represents the length of rod 2, and l_t represents the distance between the connection center of two hip joints and rod 3's gravity center. Since the leg structure of PTEXO is symmetrical, the gravity center of rod 1, 2, and 3 can be located on themselves. d_{1gc} and d_{2gc} indicate the gravity center distance of rod 1 and rod 2, respectively. d_{tgc} represents the distance between the user's torso and load gravity center in sagittal plane and the connection center of two hip joints. h_t represents the vertical distance from the user's torso and load gravity center to rod 3. θ_t represents the deviation angle of the rod 3 gravity center, which is our assumption that the addition of a load will change the original center of gravity position, and it is an adjustable (and known) setting for the wearer. θ_h and θ_k represent the hip and knee angles, respectively, measured by the magnetic encoder of SCA. Rod 1, 2, and 3 are offset from the vertical direction by angles θ_1, θ_2, and θ_3, respectively. θ_3 measured by the IMU mounted on the back of the PTEXO.

In order to calculate the accurate joint torque, the relative angle between the two bars must be used as the generalized coordinate. The coordinate transformation (2) must be performed.

$$\begin{aligned}\theta_1 &= \theta_k - \theta_h + \theta_3 \\ \theta_2 &= \theta_h - \theta_3\end{aligned} \tag{2}$$

The definitions of θ_3, θ_h, and θ_k are shown in Figure 4(a). The torque τ_h and τ_k represent the generalized force obtained from using θ_h and θ_k as generalized coordinates for the knee joint and hip joint.

The inverse dynamics equations of the swing leg were established using the model of Fig. 4(a):

$$\tau_{sw} = \begin{bmatrix}\tau_k \\ \tau_h\end{bmatrix} = \begin{bmatrix}M_{11} & M_{12} \\ M_{21} & M_{22}\end{bmatrix}\begin{bmatrix}\ddot{\theta}_k \\ \ddot{\theta}_h\end{bmatrix} + \begin{bmatrix}C_{11} & C_{12} \\ C_{21} & C_{22}\end{bmatrix}\begin{bmatrix}\dot{\theta}_k \\ \dot{\theta}_h\end{bmatrix} + \begin{bmatrix}G_1 \\ G_2\end{bmatrix} \tag{3}$$

$$M_{11} = I_1 + m_1 d_{1gc}^2$$

$$M_{12} = -I_1 - m_1 d_{1gc}^2 - m_1 d_{1gc} l_2 \cos\theta_k$$

$$M_{21} = -I_1 - m_1 d_{1gc}^2 - m_1 d_{1gc} l_2 \cos\theta_k$$

$$M_{22} = I_1 + I_2 + m_1 l_2^2 + m_1 d_{1gc}^2 + m_2 d_{2gc}^2 + 2 m_1 d_{1gc} l_2 \cos\theta_k$$

$$C_{11} = 0$$

$$C_{12} = m_1 d_{1gc} l_2 \dot{\theta}_h \sin\theta_k$$
$$C_{21} = m_1 d_{1gc} l_2 \dot{\theta}_k \sin\theta_k$$
$$C_{22} = -2m_1 d_{1gc} l_2 \dot{\theta}_k \sin\theta_k$$
$$G_1 = m_1 g d_{1gc} \sin(\theta_k - \theta_h + \theta_3)$$
$$G_2 = m_1 g l_2 \sin(\theta_h - \theta_3) + m_2 g d_{2gc} \sin(\theta_h - \theta_3) - m_1 g d_{1gc} \sin(\theta_k - \theta_h + \theta_3)$$

in which $\dot{\theta}_k$, $\dot{\theta}_h$, $\ddot{\theta}_k$, $\ddot{\theta}_h$ is the velocity, accelerations of knee and hip joint. I_i is the moment of inertia of connecting rods i, respectively.

The reference point for the support leg is chosen at the intersection of the extension of PTEXO calf bar with the ground plane. Only the motion in the sagittal plane is considered, reducing the problem to a three-link problem. Each bar is defined in the same way as the swing phase, as shown in Fig. 4(b). A coordinate transformation (4) is also required.

$$\begin{aligned} \theta_1 &= \theta_k + \theta_h + \theta_3 \\ \theta_2 &= \theta_h + \theta_3 \end{aligned} \tag{4}$$

The inverse dynamics equations of the support leg were established using the model of Fig. 4(b):

$$\tau_{st} = \begin{bmatrix} \tau_k \\ \tau_h \end{bmatrix} = \begin{bmatrix} M_{11} & M_{12} & M_{13} \\ M_{21} & M_{22} & M_{23} \end{bmatrix} \begin{bmatrix} \ddot{\theta}_k \\ \ddot{\theta}_h \\ \ddot{\theta}_3 \end{bmatrix} + \begin{bmatrix} C_{11} & C_{12} & C_{13} \\ C_{21} & C_{22} & C_{23} \end{bmatrix} \begin{bmatrix} \dot{\theta}_k \\ \dot{\theta}_h \\ \dot{\theta}_3 \end{bmatrix} + \begin{bmatrix} G_1 \\ G_2 \end{bmatrix} \tag{5}$$

$$\begin{aligned} M_{11} &= -m_t l_1 l_2 \cos\theta_k - m_t d_{tgc} l_1 \cos(\theta_h - \theta_k + \theta_t) - m_2 l_1 l_2 \cos\theta_k \\ &\quad + m_2 d_{2gc} l_1 \cos\theta_k \end{aligned}$$
$$\begin{aligned} M_{12} &= I_2 + m_t l_2^2 + m_2 l_2^2 + m_2 d_{2gc}^2 + m_t d_{tgc} l_2 \cos(\theta_h + \theta_t) - 2m_2 d_{2gc} l_2 \\ &\quad + m_t l_1 l_2 \cos\theta_k + m_t d_{tgc} l_1 \cos(\theta_h - \theta_k + \theta_t) + m_2 l_1 l_2 \cos\theta_k \\ &\quad - m_2 d_{2gc} l_1 \cos\theta_k \end{aligned}$$
$$\begin{aligned} M_{13} &= -I_2 - I_t - m_t l_2^2 - m_t d_{tgc}^2 - m_2 l_2^2 - m_2 d_{2gc}^2 \\ &\quad - m_t d_{tgc} l_1 \cos(\theta_h - \theta_k + \theta_t) - 2m_t d_{tgc} l_2 \cos(\theta_h + \theta_t) + 2m_2 d_{2gc} l_2 \\ &\quad - m_t l_1 l_2 \cos\theta_k - m_2 l_1 l_2 \cos\theta_k + m_2 d_{2gc} l_1 \cos\theta_k \end{aligned}$$
$$M_{21} = m_t d_{tgc} l_1 \cos(\theta_h - \theta_k + \theta_t)$$
$$M_{22} = -m_t d_{tgc} l_2 \cos(\theta_h + \theta_t) - m_t d_{tgc} l_1 \cos(\theta_h - \theta_k + \theta_t)$$
$$M_{23} = I_t + m_t d_{tgc}^2 + m_t d_{tgc} l_1 \cos(\theta_h - \theta_k + \theta_t) + m_t d_{2gc} l_2 \cos(\theta_h + \theta_t)$$
$$\begin{aligned} C_{11} &= -2m_t d_{tgc} l_2 \sin(\theta_h + \theta_t)\dot{\theta}_h + [-m_t d_{tgc} l_1 \sin(\theta_h - \theta_k + \theta_t) \\ &\quad + m_t l_1 l_2 \sin\theta_k + m_2 l_1 l_2 \sin\theta_k - m_2 d_{2gc} l_1 \sin\theta_k](2\dot{\theta}_3 - 2\dot{\theta}_h + \dot{\theta}_k) \end{aligned}$$
$$\begin{aligned} C_{12} &= 2m_t d_{tgc} l_2 \sin(\theta_h + \theta_t)(\dot{\theta}_3 - \dot{\theta}_h + \dot{\theta}_k) + m_t d_{tgc} l_2 \sin(\theta_h + \theta_t)\dot{\theta}_h \\ &\quad + [-m_t d_{tgc} l_1 \sin(\theta_h - \theta_k + \theta_t) + m_t l_1 l_2 \sin\theta_k + m_2 l_1 l_2 \sin\theta_k \\ &\quad - m_2 d_{2gc} l_1 \sin\theta_k](\dot{\theta}_h - 2\dot{\theta}_3) \end{aligned}$$
$$\begin{aligned} C_{13} &= [-m_t d_{tgc} l_1 \sin(\theta_h - \theta_k + \theta_t) + m_t l_1 l_2 \sin\theta_k + m_2 l_1 l_2 \sin\theta_k \\ &\quad - m_2 d_{2gc} l_1 \sin\theta_k]\dot{\theta}_3 \end{aligned}$$
$$C_{21} = 2m_t d_{tgc} l_1 \sin(\theta_h - \theta_k + \theta_t)(\dot{\theta}_k - \dot{\theta}_h + \dot{\theta}_3)$$
$$C_{22} = [m_t d_{tgc} l_1 \sin(\theta_h - \theta_k + \theta_t) + m_t d_{tgc} l_2 \sin(\theta_h + \theta_t)](\dot{\theta}_h - 2\dot{\theta}_3)$$
$$C_{23} = [m_t d_{tgc} l_1 \sin(\theta_h - \theta_k + \theta_t) + m_t d_{tgc} l_2 \sin(\theta_h + \theta_t)]\dot{\theta}_3$$
$$\begin{aligned} G_1 &= m_t g l_2 \sin(\theta_3 - \theta_h) + m_t g d_{tgc} \sin(\theta_3 + \theta_t) + m_2 g l_2 \sin(\theta_3 - \theta_h) \\ &\quad - m_2 g d_{2gc} \sin(\theta_3 - \theta_h) \end{aligned}$$
$$G_2 = -m_t g d_{tgc} \sin(\theta_3 + \theta_t)$$

in which $\dot{\theta}_3$, $\ddot{\theta}_3$ is the velocity, accelerations of the torso.

The inverse dynamics model of a lower limb exoskeleton can be summarized as (6), with $\theta = [\theta_k \quad \theta_h]^T$, $\dot{\theta} = [\dot{\theta}_k \quad \dot{\theta}_h]^T$, $\ddot{\theta} = [\ddot{\theta}_k \quad \ddot{\theta}_h]^T$ and $\tau = [\tau_k \quad \tau_h]^T$.

$$\begin{aligned} \tau_{sw} &= M_{sw}(\theta_{sw})\ddot{\theta}_{sw} + C_{sw}(\theta_{sw}, \dot{\theta}_{sw})\dot{\theta}_{sw} + G_{sw}(\theta_{sw}) \\ \tau_{st} &= M_{st}(\theta_{st})\ddot{\theta}_{st} + C_{st}(\theta_{st}, \dot{\theta}_{st})\dot{\theta}_{st} + G_{st}(\theta_{st}) \end{aligned} \tag{6}$$

The variables τ_{sw} and τ_{st} represent the joint torque in the swing phase and stance phase of PTEXO, respectively.

III. Control Strategy

To achieve a closed-loop sensitivity transfer function without measuring equivalent wearer torque directly, the inverse of the exoskeleton dynamics in Section II is used as a positive feedback controller. To address the limitations of SAC, we confidently propose ESAC. The specific extensions to SAC that constitute ESAC, including tracking differentiator, more fine-grained sensitivity factors and gait switching factor.

A. Using a Tracking Differentiator

In light of problem a), it is necessary to develop a more effective method for calculating the differential of joint angular velocity.

The Tracking Differentiator (TD) algorithm is used to obtain high-quality differential signals. The algorithm utilizes the discrete system fast optimal control synthesis function *fhan* to minimize noise in both the original signal and the differential signal. This approach also prevents high frequency chatter during digital calculations. The algorithm for tracking the differentiator is as (7):

$$\begin{cases} fh = fhan(e_1(k-1) - e_0(k), e_2(k-1), r, h_0) \\ e_1(k) = e_1(k-1) + h \cdot e_2(k-1) \\ e_2(k) = e_2(k-1) + h \cdot fh \end{cases} \tag{7}$$

Where $e_0(k)$ is the input position signal sequence, $e_1(k)$ is the output position tracking signal (or filter signal) of $e_0(k)$, $e_2(k)$ is the output velocity differential signal (or derivative signal) of $e_1(k)$, then $fh(\cdot)$ is the calculated optimal acceleration. r is the speed factor for tracking speed, h_0 is the filter factor, and h is the integral step calculated by the digital controller. The definition of $fhan(\cdot)$ can be found in [25].

B. Fine-grained Sensitivity Amplification Factors

In response to problem b), more precise amplification coefficients are designed for the inertial force term and the centrifugal force and Coriolis force term. By introducing amplification coefficients α_{Msw} and α_{Mst} for the sensitivity of the inertial terms of the swing and stance phases, and α_{Csw} and α_{Cst} for the sensitivity of the centripetal Koch terms of the swing and stance phases, the calculation equation of the control command can be transformed into (8):

$$\begin{aligned} \tau_{sw} &= (1 - \alpha_{Msw}^{-1})M_{sw}(\theta_{sw})\ddot{\theta}_{sw} + (1 - \alpha_{Csw}^{-1})C_{sw}(\theta_{sw}, \dot{\theta}_{sw})\dot{\theta}_{sw} + G_{sw}(\theta_{sw}) \\ \tau_{st} &= (1 - \alpha_{Mst}^{-1})M_{st}(\theta_{st})\ddot{\theta}_{st} + (1 - \alpha_{Cst}^{-1})C_{st}(\theta_{st}, \dot{\theta}_{st})\dot{\theta}_{st} + G_{st}(\theta_{st}) \end{aligned} \tag{8}$$

The control system addresses the issue of differing sensitivity between the speed and acceleration signals. It generates a control command that is better suited for the actual working conditions of the lower limb exoskeleton robot. The lower extremity exoskeleton control system is highly sensitive

to changes in acceleration signals. Therefore, the amplification coefficient is typically set according to the rule of $\alpha_{Msw} < \alpha_{Csw}$ and $\alpha_{Mst} < \alpha_{Cst}$.

C. Gait Switching Factor

The inverse dynamics model varies depending on whether the exoskeleton legs are in the swing phase or the support phase [26]. Therefore, it is important to determine the current gait phase and establish the conditions for switching the control law of the lower limb exoskeleton between different inverse dynamics models. The common practice is to set a pressure threshold of ε_p for plantar pressure [27]. It is believed that when the plantar pressure F_p is less than ε_p, the leg is in the swing phase. When the plantar pressure F_p is greater than or equal to ε_p, the leg is in the support phase. By setting the left plantar pressure of the lower limb exoskeleton as F_{pL} and the right plantar pressure as F_{pR}, a gait phase division table for the lower limb exoskeleton can be established (Table I).

TABLE I.
GAIT PHASE DIVISION BASED ON A SINGLE THRESHOLD OF PLANTAR PRESSURE.

Sensor status	$F_{pR} < \varepsilon_p$	$F_{pR} \geq \varepsilon_p$
$F_{pL} < \varepsilon_p$	Remove PTEXO	Stance phase[a]
$F_{pL} \geq \varepsilon_p$	Swing phase[a]	Double-stance phase

a. Take the right leg gait phase as an example. And the left leg gait phase is opposite.

A joint torque defined in (9) expression for any leg of the PTEXO can be generated based on Table I:

$$\tau = \begin{cases} \tau_{sw}, & F_p < \varepsilon_p \\ \tau_{st}, & F_p \geq \varepsilon_p \end{cases} \tag{9}$$

For problem c), a transition process must be arranged between the swing phase and the stance phase of the single leg. We developed a gait phase switching algorithm to determine the gait switching factor β, as well as the swing phase pressure threshold ε_{sw} and support phase pressure threshold ε_{st}. The final joint torque of the PTEXO is as (10):

$$\tau = \beta\tau_{st} + (1-\beta)\tau_{sw} \tag{10}$$

And the calculation method for the gait switching factor β is as (11):

$$\beta = \begin{cases} 1, & F_p \geq \varepsilon_{st} \\ (F_p - \varepsilon_{sw}) / (\varepsilon_{st} - \varepsilon_{sw}), & \varepsilon_{sw} \leq F_p < \varepsilon_{st} \\ 0, & F_p < \varepsilon_{sw} \end{cases} \tag{11}$$

When PTEXO is in the double-stance phase, both legs are fully in the stance phase. When the wearer removes PTEXO, the controller will immediately reset the output torque commands for each motor. The motors do not provide any torque until the system hits the ground. If the wearer dismounts the exoskeleton robot, the withdrawal of torque prevents the robot from behaving uncontrollably without feedback from the wearer. This configuration significantly enhances the safety of the PTEXO.

These are the improved aspects of the Enhanced Sensitivity Amplification Control (ESAC) strategy, and the overall framework of the control system is shown in Fig. 5.

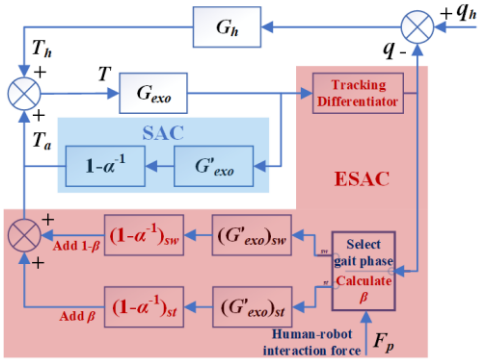

Fig. 5. SAC (blue) and ESAC (red) control strategy block diagram.

G_h represents the inverse dynamic transfer function of the human body; G_{exo} represents the true dynamic transfer function of PTEXO. Fp stands for plantar pressure, that is, human-robot interaction. It is used to judge and divide gait phase. G'_{exo} is the inverse dynamics model of PTEXO embedded in the MCU. The selection of the supporting or swinging model is selected according to the gait phase judgment. α is the sensitivity amplification factor of the system, which can be divided into swinging phase coefficients (α_{Msw} and α_{Csw}) and supporting phase coefficients (α_{Mst} and α_{Cst})by gait phase. q represents the motion state of each joint of PTEXO, including the angle, angular velocity, and angular acceleration. q_h represents the motion state of each joint of the wearer's lower limbs; T_h represents the interaction torque between PTEXO and the human body, converted to each joint; T_a represents the torque provided by the actuator on each joint of PTEXO; T represents the combined torque of each joint of PTEXO.

IV. EXPERIMENTS AND RESULTS DISCUSSION

A. Tracking Differentiator Experiment and Discussion

This first experiment evaluates how the TD and baseline differential trackers affect the smoothness of the generated angular acceleration signals. The ESAC algorithm uses a TD to track the angular acceleration signals of the joints. This improves the accuracy of input for computing the inverse dynamics model. This experiment conducted on the PTEXO involved measuring the angles and angular velocities of the hip and knee joints of both legs using the actuator's magnetic encoder. Differential and TD algorithms are implemented using MATLAB. The signals for angular acceleration were processed and plotted, as shown in Fig. 6.

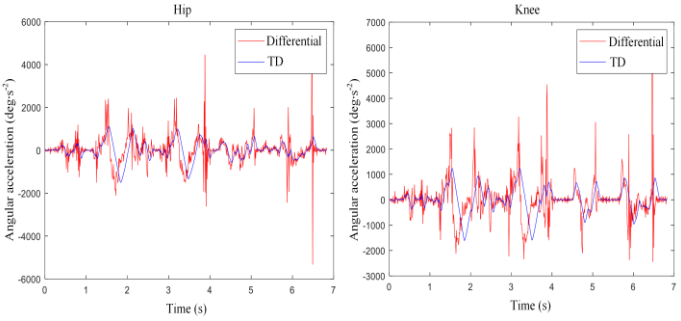

Fig. 6. Comparison of angular acceleration calculated by difference algorithm and TD algorithm.

The TD algorithm significantly reduces the degree of jitter and the number of spikes in the joint angular acceleration signals, compared to the results obtained from the differential method. The quality of the joint angular acceleration signals calculated by the TD algorithm is significantly higher than that of the differential method. Therefore, it can be concluded that using the TD algorithm to obtain the necessary joint angular acceleration for generating control commands is a superior option.

B. Gait Switching Factor Experiment and Discussion

This second experiment evaluates how the SAC with a gait-switching factor β and baseline SAC algorithms affect the smoothness of the generated joint torque control commands. Pressure data was collected from the soles of both feet during the walking test. The control algorithm code, which includes a gait switching factor β, and an original SAC algorithm code were written in MATLAB to test the data for the same walking. The time period when the gait phase switching occurs is selected, and the generated torque control instructions are compared, as shown in Fig. 7.

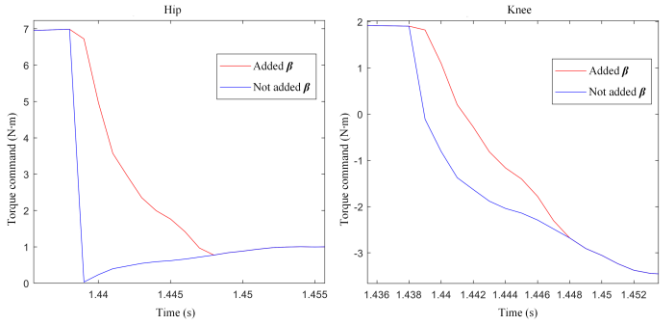

Fig. 7. Comparison of joint torque control commands for the right leg during the transition from swing phase to stance phase.

After incorporating the gait switching factor β, the moment control commands for the hip and knee joints show improved continuity and smoothness compared to the inverse dynamics model switching SAC method without β. β is added to prevent sudden changes in the torque commands received by the active joints of PTEXO. This greatly improves the stability of the control system, enhances the wearer's walking experience and increases the reliability and fluency of PTEXO.

C. Wearable Experiment and Discussion

This third experiment evaluates the performance of motion following and assisting effect of PTEXO using SAC and ESAC strategy. The assisted lower-limb exoskeleton should have two main functions: bearing heavy loads for the wearer and effectively following the user's autonomous movement. A 15kg barbell is secured to the back of the PTEXO trunk using a nylon strap. After activating PTEXO, the wearer performs walking and squatting exercise tests with and without a loaded barbell, as shown in Fig. 8(a). And our plantar pressure sensors are mounted on the foot surface of the exoskeleton, as shown in Fig. 8(b). The data collected by the sensors is the Interaction Force (IF) of the exoskeleton robot in contact with a human, with zero indication when there is no user wearing it. The IF reflects the weight of the user plus the amount of load acting on user's body, and can evaluate the degree to which PTEXO reduce the burden on body.

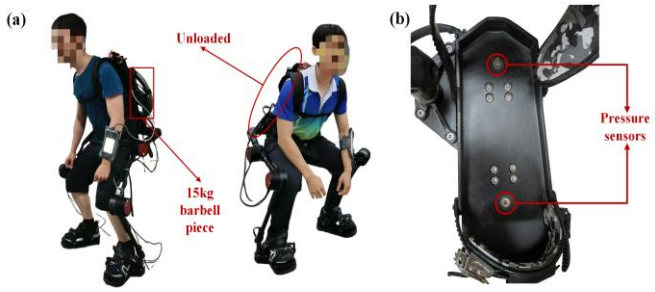

Fig. 8. Actual photographic: (a) Experiments on the motion of the PTEXO robot with and without load. (b) Installation site for plantar pressure sensors.

The torque data of the actuator in response to control commands was collected from the wearer using the PTEXO during weight-bearing walking, as shown in Fig. 9. In this test, the tester performs a walking movement from 0s to 10s and then transitions to a squatting movement in place after 10s. The torque generated by the motors on the four active joints of the PTEXO accurately follows the torque control instructions generated by the control algorithm. Proved that PTEXO can effectively follow the user's autonomous movement. One more thing, the foot structure of the PTEXO collides with the ground upon landing, causing an impact on the leg joints. This impact leads to spikes and burrs in the force experienced by the active joints.

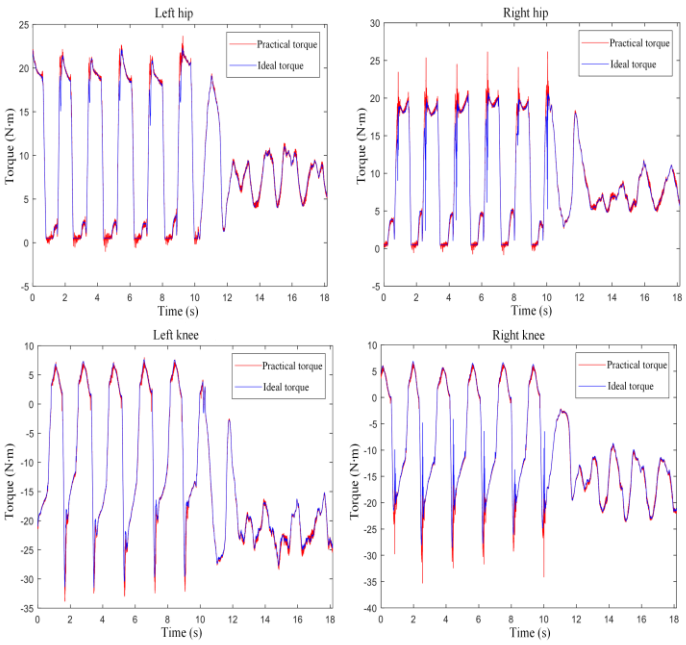

Fig. 9. Joint torque tracking diagram.

We chose the left hip joint of PTEXO as an object and compared the ESAC and SAC to generate the actual moments, and the results are shown in Fig. 10. The results show that the baseline SAC without any extension has relatively large jitter when generating the practical torque, especially when switching the gait phase and motion modes of PTEXO. And ESAC, on the other hand, suppresses this jitter well. Controlling the torque jitter and overshooting is something we do not want to see, because it not only causes discomfort to the user during motion, but also consumes extra energy and reduces the endurance time. Meanwhile, the comparison results prove the advantage of our ESAC strategy, which is to suppress the control torque jitter.

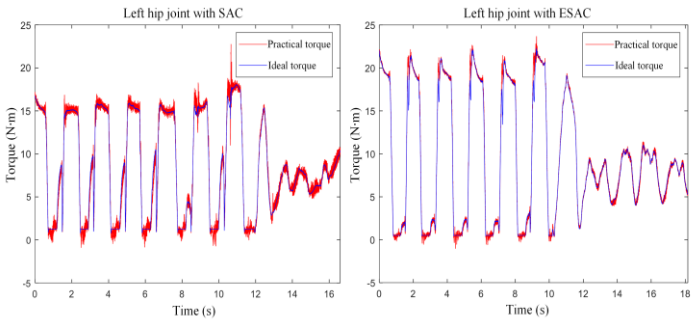

Fig. 10. Comparison of SAC and ESAC strategy for generating practical torque.

In load-bearing situations, the PTEXO provides a noticeable assisting effect to the human body. This is because the load is only fixed to the back structure of the PTEXO, and the PTEXO generates enough driving force in the sagittal plane to compensate for the extra load. From a macroscopic perspective, the load force on the back of the PTEXO is transmitted to the ground through its back, leg, and foot structure, in that order. It can be assumed that there is minimal additional force loaded on the wearer.

This can be confirmed by analyzing the plantar pressure of the same wearer (body weight 86.8kg) during walking with and without PTEXO, both unloaded and loaded tests. In the walking test, due to the symmetry of gait cycle, two feet move in alternating phases, but the amplitude of left and right plantar pressures are equal, so it is sufficient to take one of plantar pressures to analyze the force. Here, we take the plantar pressure of right foot, as depicted in Fig. 11. 1) When unloaded without PTEXO, the plantar pressure is about 850N, which is the user's own weight. It plus a 15kg load to reach around 1000N. 2) When unloaded with PTEXO power off, the pressure is about 1125N, which is caused by the weight of PTEXO loading on the user. It reaches around 1275N when loaded. 3) When loaded with PTEXO power on, compared with the unloaded situation, the user's plantar pressure did not change much, and both were near 850N. This indicates that most of the load force from a 15kg barbell is conducted to the ground via PTEXO without being loaded onto the user's body, proving that PTEXO can effectively assist the wearer.

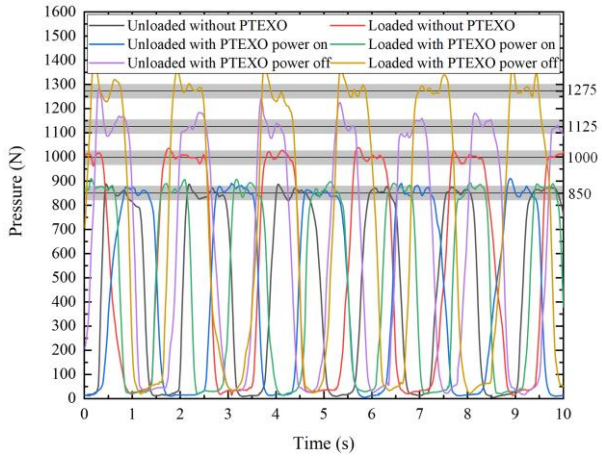

Fig. 11. Comparison of plantar pressure in unloaded and loaded tests.

In addition, a user survey was done. A total of 10 healthy participants (8 males 2 females, mean age 28 years) were asked to participate in the experiment. Informed consent was obtained from all subjects. The experimental protocol applied in this study was approved by the ethics committee in School of Automation Science and Electrical Engineering, Beihang University and we followed the ethical standards laid down in the Declaration of Helsinki. During the experiment, participants were asked to perform upright walking and squatting maneuvers wearing PTEXO with a loaded barbell in a blinded comparison of SAC vs. ESAC. Just after each trial, participants answered the following questions: Q1. I felt assisted and smooth and light; Q2. I felt assisted but also stuttered and hindered; Q3. I did not feel assisted and was burdensome. Q1 and Q2 are designed to evaluate SAC and ESAC. Q3 is designed to verify whether participants have experienced effective help. A seven-point Likert scale was applied to assess how much the participants agree to the statements. In this survey, 1 and 7 meant "I strongly disagree with the statement" and "I strongly agree with the statement", respectively; the intermediate scores were freely compensated by participants. We can maintain that the lower the Q3 score, the better the assistance effect. If a strategy has a significantly higher Q1 score than Q2, then this strategy is smoother and more comfortable.

Fig. 12 shows the average scores over 10 participants as bar chart with the standard error of mean (SEM). As expected, in terms of average scores, there was little difference between ESAC and SAC in Q3, with both scores at the lower end of the scale, suggesting that they both lighten the load on the body. The predominance of ESAC scores in Q1 and SAC scores in Q2 reflects the fact that ESAC is smoother and more comfortable than SAC.

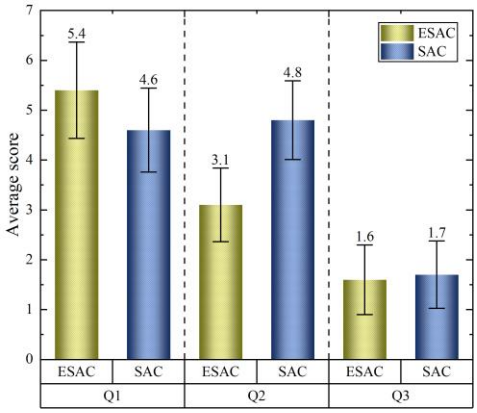

Fig. 12. Results of the SAC vs. ESAC questionnaire in walking task given by a seven-point Likert scale. Bar charts and error bars show the average scores over 10 participants and the SEMs.

D. Limitation

1) Since PTEXO only has the force interaction mode of plantar pressure, it cannot obtain the human-robot interaction force in all directions at the straps. It is necessary to add multidimensional force sensors to measure interaction forces in all directions at the straps in order to assess the "transparency" of wearable exoskeletons. 2) PTEXO cannot complete the automatic identification of load conditions, such as the shape, volume, and weight of the load. The shape and volume of the load will affect the overall gravity center position of PTEXO, which may make the error of algorithm model larger, resulting in poor assistance effect. It is necessary to develop a function that automatically obtains gravity center position after the load is loaded into PTEXO, so that the

parameters of algorithm model regarding gravity center position can be adjusted in real time, thus ensuring efficient assistance. 3) PTEXO is a principle prototype, limited by the torque performance of SCA, not applicable to the oversized load situation (refers to a situation in which the assist required for load exceeds the maximum assist torque that can be provided by the joint actuators, resulting in assist failure). It is necessary to develop a function to recognize the weight of the load, so that when the load reaches the torque threshold, the system issues an alarm to indicate that there is danger. These limitations will be improved in the future work.

V. Conclusion

In this work, we develop a wearable exoskeleton robot for enhancing lower limb function. The robot's dynamics are modeled, and an ESAC strategy is proposed to enhance system smoothness and reliability. Our Enhanced SAC (ESAC) method improves upon the traditional SAC method by obtaining high-quality angular acceleration signals, compensating for system instability caused by errors in the dynamics model, and enhancing the wearer's motion experience during gait switching. The results of wearer experiments and the user survey confirm the stability and effectiveness of the ESAC strategy. However, the PTEXO shadowing the users is the ideal case. PTEXO with its limitations is getting close to this ideal case.

References

[1] J. L. Pons, *Wearable Robots: Biomechatronic Exoskeletons*. New York, John Wiley & Sons, Ltd, 2008, pp. 1–15.

[2] T. Yan, M. Cempini, C. M. Oddo, and N. Vitiello, "Review of assistive strategies in powered lower-limb orthoses and exoskeletons," *Robotics and Autonomous Systems*, vol. 64, pp. 120–136, 2015, doi: 10.1016/j.robot.2014.09.032.

[3] S. Qiu, Z. Pei, C. Wang, and Z. Tang, "Systematic Review on Wearable Lower Extremity Robotic Exoskeletons for Assisted Locomotion," *Journal of Bionic Engineering*, vol. 20, pp. 436–469, 2023, doi: 10.1007/s42235-022-00289-8.

[4] W. Sun, J.-W. Lin, S.-F. Su, N. Wang, and M. J. Er, "Reduced adaptive fuzzy decoupling control for lower limb exoskeleton," *IEEE Trans. Cybern.*, vol. 51, no. 3, pp. 1099–1109, Mar. 2021.

[5] A. Martinez, B. Lawson, and M. Goldfarb, "A controller for guiding leg movement during overground walking with a lower limb exoskeleton," *IEEE Trans. Robot.*, vol. 34, no. 1, pp. 183–193, Feb. 2018.

[6] U. E. Ogenyi, J. Liu, C. Yang, Z. Ju, and H. Liu, "Physical human–robot collaboration: Robotic systems, learning methods, collaborative strategies, sensors, and actuators," *IEEE Trans. Cybern.*, vol. 51, no. 4, pp. 1888–1901, Apr. 2021.

[7] C. Camardella, F. Porcini, A. Filippeschi, S. Marcheschi, M. Solazzi and A. Frisoli, "Gait Phases Blended Control for Enhancing Transparency on Lower-Limb Exoskeletons," *IEEE Robotics and Automation Letters*, vol. 6, no. 3, pp. 5453-5460, July 2021, doi: 10.1109/LRA.2021.3075368.

[8] Z. Li, *et al*., "Human-in-the-Loop Control of a Wearable Lower Limb Exoskeleton for Stable Dynamic Walking," *IEEE/ASME Transactions on Mechatronics*, vol. 26, no. 5, pp. 2700-2711, Oct. 2021, doi: 10.1109/TMECH.2020.3044289.

[9] J. Zhang, *et al*., "Human-in-the-loop optimization of exoskeleton assistance during walking," *Science*, vol. 356, pp. 1280-1284, 2017, doi: 10.1126/science.aal5054.

[10] B. Hu, J. Xue, D. Jiang, *et al.*, "Wearable Exoskeleton System for Energy Harvesting and Angle Sensing Based on a Piezoelectric Cantilever Generator Array," *ACS Applied Materials & Interfaces,* vol.14, no. 32, pp. 36622-36632, 2022, doi: 10.1021/acsami.2c08757.

[11] J. Song, A. Zhu, Y. Tu, H. Mao and X. Zhang, "Adaptive neural fuzzy reasoning method for recognizing human movement gait phase," *Robotics and Autonomous Systems,* vol.153, pp. 104087, 2022, doi: 10.1016/j.robot.2022.104087.

[12] L. Ferrero, V. Quiles, M. Ortiz, *et al.*, "Brain-computer interface enhanced by virtual reality training for controlling a lower limb exoskeleton," *iScience,* vol. 26, Issue 5, pp. 106675, 2023, doi: 10.1016/j.isci.2023.106675.

[13] S. R. Soekadar *et al*., "Hybrid EEG/EOG-based brain/neural hand exoskeleton restores fully independent daily living activities after quadriplegia," *Science Robotics,* vol. 1, no. 1, pp. eaag3296, 2016, doi: 10.1126/scirobotics.aag3296.

[14] C. Shen, Z. Pei, W. Chen, J. Wang, J. Zhang and Z. Chen, "Toward Generalization of sEMG-Based Pattern Recognition: A Novel Feature Extraction for Gesture Recognition," *IEEE Transactions on Instrumentation and Measurement,* vol. 71, pp. 1-12, 2022, Art no. 2501412, doi: 10.1109/TIM.2022.3141163.

[15] C. Shen, Z. Pei, W. Chen, J. Wang, X. Wu and J. Chen, "Lower Limb Activity Recognition Based on sEMG Using Stacked Weighted Random Forest," *IEEE Transactions on Neural Systems and Rehabilitation Engineering,* vol. 32, pp. 166-177, 2024, doi: 10.1109/TNSRE.2023.3346462.

[16] J.-L. C. Racine, "Control of a lower extremity exoskeleton for human performance amplification," Ph.D. dissertation, Dept. Mechanical. Eng., University of California, Berkeley, CA: U. C. Berkeley, 2003.

[17] R. Steger, Sung Hoon Kim and H. Kazerooni, "Control scheme and networked control architecture for the Berkeley lower extremity exoskeleton (BLEEX)," in *Proc. IEEE International Conference on Robotics and Automation,* Orlando, FL, 2006, pp. 3469-3476, doi: 10.1109/ROBOT.2006.1642232.

[18] R. Bogue, "Exoskeletons and robotic prosthetics: A review of recent developments," *Industrial Robot-The International Journal of Robotics Research and Application,* vol. 36, no. 5, pp. 421–427, 2009, doi: 10.1108/01439910910980141.

[19] H. Kazerooni, N. H. Harding, and R. Angold, "Lower extremity exoskeleton," United State Patent, Application Publication, US7947004B2, 2011.

[20] H. Kim, Y. J. Shin and J. Kim, "Design and locomotion control of a hydraulic lower extremity exoskeleton for mobility augmentation," *Mechatronics,* vol. 46, pp. 32-45, Oct. 2017.

[21] S. De Groof, Y. Zhang, L. Peyrodie and L. Labey, "Design and Control of an Individualized Hip Exoskeleton Capable of Gait Phase Synchronized Flexion and Extension Torque Assistance," in *IEEE Access,* vol. 11, pp. 96206-96220, 2023, doi: 10.1109/ACCESS.2023.3311352.

[22] J. Liu and Y. He and J. Yang et al., "Design and analysis of a novel 12-DOF self-balancing lower extremity exoskeleton for walking assistance," *Mechanism and Machine Theory,* vol. 167, pp. 104519, 2022, doi: 10.1016/j.mechmachtheory.2021.104519.

[23] Musculoskeletal Key-Fastest Musculoskeletal Insight Engine. Available online: https://musculoskeletalkey.com/gait-and-posture-analysis/ (accessed on 27 February 2024)

[24] Y. Chen, Z. Li, H. Kong and F. Ke, "Model Predictive Tracking Control of Nonholonomic Mobile Robots With Coupled Input Constraints and Unknown Dynamics," *IEEE Transactions on Industrial Informatics*, vol. 15, no. 6, pp. 3196-3205, June 2019, doi: 10.1109/TII.2018.2874182.

[25] J. Han, "From PID to Active Disturbance Rejection Control," *IEEE Transactions on Industrial Electronics,* vol. 56, no. 3, pp. 900-906, March 2009, doi: 10.1109/TIE.2008.2011621.

[26] M. Lee, J. Kim, S. Hyung, *et al.*, "A Compact Ankle Exoskeleton With a Multiaxis Parallel Linkage Mechanism," *IEEE/ASME Transactions on Mechatronics,* vol. 26, no. 1, pp. 191-202, Feb. 2021, doi: 10.1109/TMECH.2020.3008372.

[27] B. Ren, J. Liu, W. Guan, *et al.*, "Gait phase recognition of multi-mode locomotion based on multi-layer perceptron for the plantar pressure measurement system," *International Journal of Intelligent Robotics and Applications,* vol. 7, pp. 602–614, 2023, doi: 10.1007/s41315-023-00283-1.